

Engineering a Rugged Nanoscaffold To Enhance Plug-and-Display Vaccination

Theodora U. J. Bruun,^{†,§} Anne-Marie C. Andersson,^{†,§} Simon J. Draper,[‡] and Mark Howarth^{*,†,‡,§}

[†]Department of Biochemistry, University of Oxford, South Parks Road, Oxford OX1 3QU, United Kingdom

[‡]Jenner Institute, University of Oxford, Oxford OX3 7DQ, United Kingdom

S Supporting Information

ABSTRACT: Nanoscale organization is crucial to stimulating an immune response. Using self-assembling proteins as multimerization platforms provides a safe and immunogenic system to vaccinate against otherwise weakly immunogenic antigens. Such multimerization platforms are generally based on icosahedral viruses and have led to vaccines given to millions of people. It is unclear whether synthetic protein nanoassemblies would show similar potency. Here we take the computationally designed porous dodecahedral i301 60-mer and rationally engineer this particle, giving a mutated i301 (mi3) with improved particle uniformity and stability. To simplify the conjugation of this nanoparticle, we employ a SpyCatcher fusion of mi3, such that an antigen of interest linked to the SpyTag peptide can spontaneously couple through isopeptide bond formation (Plug-and-Display). SpyCatcher-mi3 expressed solubly to high yields in *Escherichia coli*, giving more than 10-fold greater yield than a comparable phage-derived icosahedral nanoparticle, SpyCatcher-AP205. SpyCatcher-mi3 nanoparticles showed high stability to temperature, freeze–thaw, lyophilization, and storage over time. We demonstrate approximately 95% efficiency coupling to different transmission-blocking and blood-stage malaria antigens. *Plasmodium falciparum* CyRPA was conjugated to SpyCatcher-mi3 nanoparticles and elicited a high avidity antibody response, comparable to phage-derived virus-like particles despite their higher valency and RNA cargo. The simple production, precise derivatization, and exceptional ruggedness of this nanoscaffold should facilitate broad application for nanobiotechnology and vaccine development.

KEYWORDS: *bionanotechnology, nanomedicine, vaccination, protein engineering, bioconjugation, virus-like particle, self-assembly*



Nanoassembly creates great opportunities for studying and modulating biological systems.^{1–3} Decorating functional units onto nanoparticles can enhance function in areas including catalysis,^{4,5} imaging,⁶ and therapy.⁷ Protein-based nanoparticles, compared to abiotic synthetic polymers, may have the advantage of atomically precise assembly, but at the cost of low stability and difficulty in scaling up production.^{8,9} Exploiting the natural immunogenicity of proteinaceous cages as well as the multimerization of antigens is crucially important to the development of the next generation of vaccines.^{10,11} Developing a modular and robust nanoscaffold with scalable, low-cost production could contribute to major challenges in human and animal health,¹² including vaccines to rapidly evolving pathogens (e.g., HIV, malaria) or zoonotic outbreaks (e.g., Ebola virus, Rift Valley fever). Such a platform would also be important for vaccine stockpiling against pandemics and for vaccine delivery to low-resource areas.^{13,14}

Traditional vaccines based on whole-killed or live-attenuated viruses are good at stimulating immune responses but pose a greater risk of rare adverse events.^{15,16} Recombinant subunit vaccines, while safer, are often insufficiently immunogenic to progress through clinical development.^{17–20} By using virus-like

particles (VLPs) as multimerization platforms, antigens can be delivered to the immune system on a highly immunogenic scaffold in a safe fashion.¹⁰ The immunogenicity of VLPs is a product of efficient draining to lymph nodes, efficient uptake by dendritic cells, and a highly repetitive surface that promotes B-cell cross-linking and activation.^{21–24}

Conjugation of antigens onto a VLP or nanoparticle can be achieved through a variety of techniques including chemical conjugation,²⁵ genetic fusion,^{26,27} or bio-orthogonal chemistry with unnatural amino acids.²⁸ Genetic fusion frequently runs into difficulty from inefficient folding of complex antigens.^{29–31} Chemical coupling faces challenges from the heterogeneity in coupling site and particle coverage.³² We recently established another method for VLP decoration, exploiting the spontaneous isopeptide bond that forms between the protein domain SpyCatcher and its peptide partner SpyTag.¹⁸ This ability to separate antigen and scaffold production through modular assembly, termed “Plug-and-Display” (Figure 1a), allows

Received: April 14, 2018

Accepted: July 20, 2018

Published: July 20, 2018

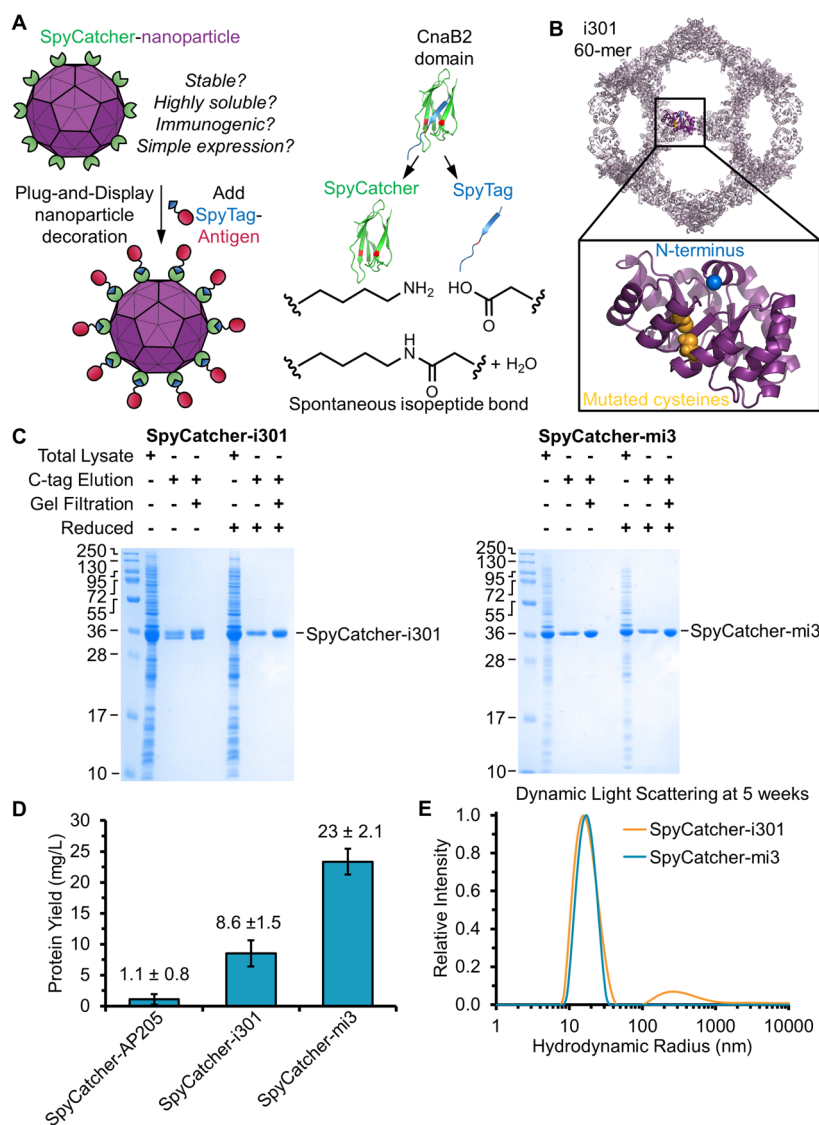


Figure 1. Design principle of rugged nanoscaffold platform. (a) Cartoon showing Plug-and-Display decoration of SpyCatcher-nanoparticles with a SpyTag-antigen and key issues for a robust platform. (b) Modification of the i301 scaffold. Two surface-exposed cysteines, C76 and C100 in i301 (yellow), were mutated to alanine to produce the mi3 nanoparticle platform. i301 is shown as the intact 60-mer and inset as a single monomer (based on the designed structure PyMOL file). The N-terminus is highlighted in blue. (c) mi3 increased the uniformity of the purified protein. Induction and purification gel, showing the additional disulfide-bonded species present for SpyCatcher-i301 but not SpyCatcher-mi3, analyzed by SDS-PAGE with Coomassie staining. (d) mi3 enhanced nanoscaffold yield. Purified protein yield (mean \pm 1 s.d., $n = 3$) was compared for SpyCatcher-mi3, SpyCatcher-i301, and SpyCatcher-AP205. (e) SpyCatcher-mi3 showed greater stability to aggregation. SpyCatcher-i301 or SpyCatcher-mi3 were stored for 5 weeks at 4 °C and analyzed by DLS.

optimization of production conditions for both components and may shorten time from development to manufacture of a new vaccine.³³ These Plug-and-Display platforms were based on SpyTag or SpyCatcher linked to the coat protein cp3 from the bacteriophage AP205. Spy-AP205 VLPs have been investigated as vaccine candidates against a number of targets, including malaria and cancer.^{18,34,35} However, despite the fact that Spy-AP205 VLPs are good at stimulating the immune system, a number of concerns hinder their clinical development, including limited solubility, stability, and yield (Figure 1a).

Protein cages from both nonviral and viral origin have gained increased interest expanding on possible applications in the fields of vaccine technology and biotechnology.^{36–38} Recently, protein nanocages that mimic the structure of VLPs have been computationally designed, although their

immunogenicity remains untested.³⁹ The i301 nanocage is based on the 2-keto-3-deoxy-phosphogluconate (KDPG) aldolase from the Entner–Doudoroff pathway of the hyperthermophilic bacterium *Thermotoga maritima*. i301 has five mutations that alter the interface between the wild-type protein trimer, promoting assembly into a higher order dodecahedral 60-mer (Figure 1b). In this paper we use rational design to improve i301 stability and establish modular antigen coupling by fusing SpyCatcher to the N-terminus of the protein. We then characterize the conformation, ruggedness, and immunogenicity of the SpyCatcher-mi3 scaffold to evaluate its potential to accelerate vaccine development.

RESULTS AND DISCUSSION

To create a Plug-and-Display nanoscaffold, Δ N1-SpyCatcher was genetically fused to the N-terminus of the previously

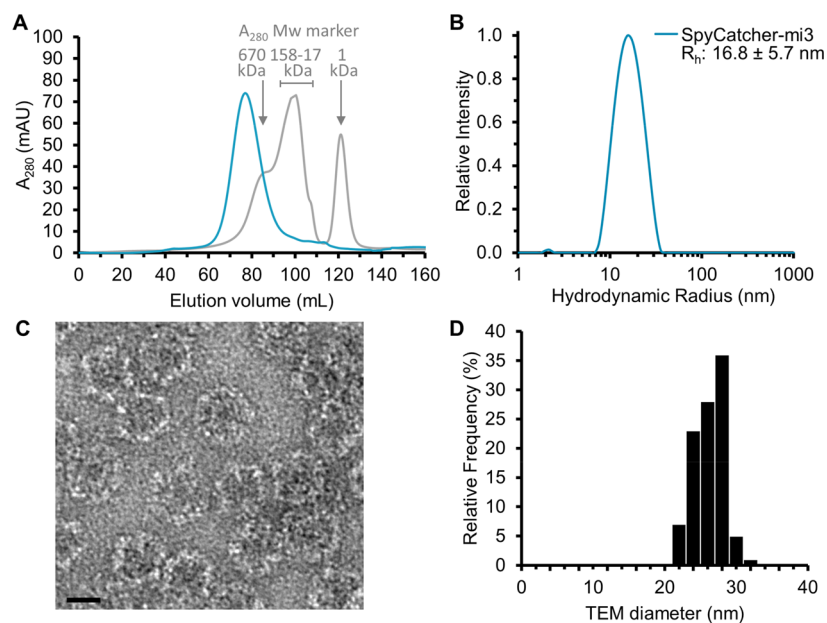


Figure 2. Biophysical characterization of SpyCatcher-mi3 nanoparticles. (a) Size-exclusion chromatography of SpyCatcher-mi3 showed assembly into nanoparticles by absorbance at A_{280} (blue line), with comparison to molecular weight markers (gray line). (b) DLS determination of hydrodynamic radius (R_h) of SpyCatcher-mi3. (c) Negatively stained TEM image of SpyCatcher-mi3 nanoparticles. Scale bar 25 nm. (d) Size distribution of SpyCatcher-mi3 nanoparticles from TEM ($n = 100$).

described i301 sequence.³⁹ A C-tag was installed on the C-terminus to allow more efficient downstream processing for vaccine applications.^{40,41} This construct expressed solubly in *E. coli*, and particles were purified from cell lysate by C-tag resin affinity chromatography followed by size-exclusion chromatography (Figure 1c). We found difficulties during purification arising from aggregation of the cell lysate. We also saw a double-banded SpyCatcher-i301 product by SDS-PAGE, which converted to a single band upon reduction, indicative of intrachain disulfide bond formation (Figure 1c). Therefore, we designed mutations of two surface-exposed cysteines C76A and C100A (Figure 1b, Supporting Information, Figure S1a) to avoid potential disulfide bond-mediated heterogeneity. Evidence from sequence conservation of KDPG aldolases indicates that alanine is the preferred amino acid at position 76 (Supporting Information, Figure S1b). Removing complicating disulfide bond formation or the need for the presence of reducing agent³⁹ would also assist the conjugation of many antigens that require intact disulfide bonds. We termed this mutated i301 sequence mi3. SpyCatcher-mi3 was efficiently purified under the same conditions, with no double-banded species visible by SDS-PAGE (Figure 1c).

After purification, SpyCatcher-mi3 gave 2-fold higher yield than SpyCatcher-i301 (Figure 1d). This yield is more than 10-fold higher than we could achieve for SpyCatcher-AP205, despite extensive optimization of DNA constructs, bacterial strains, and conditions for growth and induction (Figure 1d).¹⁸ 23 mg/L is close to the maximum we achieve for any soluble protein in shake-flask *E. coli* culture.^{20,42,43} Higher yields should be accessible through fermentation.⁴⁴

The mutations in SpyCatcher-mi3 also eliminated the aggregation of SpyCatcher-i301 seen by dynamic light scattering (DLS) after 5 weeks of storage (Figure 1e). Therefore, all further studies were performed with SpyCatcher-mi3.

Size-exclusion chromatography of SpyCatcher-mi3 showed a single major peak eluting in the expected megadalton range (a monomer of SpyCatcher-mi3 is 34 kDa, the 60-meric nanoparticle MW is estimated at $60 \times 34 \text{ kDa} = 2.0 \text{ MDa}$) (Figure 2a). On this trace we also observed the elution of lower molecular weight species (in the range of 1–158 kDa based on the marker), which are likely unassembled monomeric or trimeric species (Figure 2a) and were removed by our size-exclusion purification. Quantifying purified SpyCatcher-mi3 nanoparticles by DLS gave a uniform peak of the hydrodynamic radius (R_h) $16.8 \pm 5.7 \text{ nm}$ (Figure 2b). Negative-staining transmission electron microscopy (TEM) of SpyCatcher-mi3 indicated assembly of the expected dodecahedra (Figure 2c), with a diameter of $26 \pm 2.0 \text{ nm}$ (mean ± 1 s.d., $n = 100$) (Figure 2d). As expected, this size is smaller than the hydrodynamic size from DLS.

To validate SpyCatcher-mi3 reactivity, we performed initial trials with the model protein SpyTag-MBP (*E. coli* maltose-binding protein).⁴⁵ Upon mixing with excess SpyTag-MBP, a clear SpyCatcher-mi3 molecular weight band shift was observed on SDS-PAGE, indicating covalent bond formation (Figure 3a). The reaction proceeded to 91% conjugation after 16 h at 25 °C (Supporting Information, Figure S2a). We tested conjugation of SpyCatcher-mi3 to immunologically relevant SpyTagged antigens against malaria (Figure 3b–d). Cysteine-rich interdomain region (CIDR) is a variable domain type from the parasite *Plasmodium falciparum* erythrocyte membrane protein-1 family (PfEMP1).⁴⁶ Pfs25 is a malaria transmission-blocking antigen that has shown promise in previous vaccine trials.^{17,47,48} Cysteine-rich protective antigen (CyRPA) is involved in *P. falciparum* merozoite invasion into erythrocytes. CyRPA is highly conserved and is another promising malaria vaccine candidate.^{49,50} These antigens were conjugated to SpyTag at either the N-terminus (CIDR) or the C-terminus (Pfs25 and CyRPA). Antigens were expressed in *E. coli* (SpyTag-CIDR, 30 kDa, 4 disulfide bonds) or mammalian

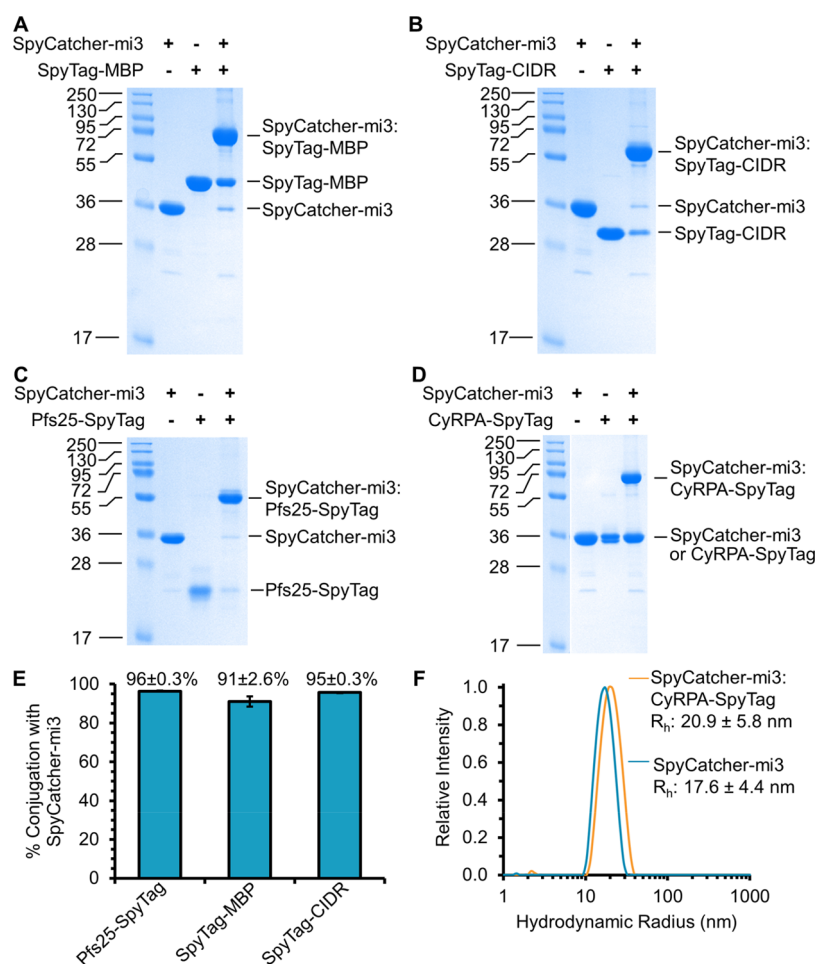


Figure 3. SpyCatcher-mi3 nanoparticles efficiently reacted with a variety of antigens. Conjugation was performed with SpyCatcher-mi3 in a 1:3 ratio with antigen at 25 °C for 16 h, followed by analysis on SDS-PAGE with Coomassie staining. (a) SpyTag-MBP. (b) SpyTag-CIDR. (c) Pfs25-SpyTag. (d) CyRPA-SpyTag. (e) Coupling efficiency of SpyCatcher-mi3 with antigens, quantified by SDS-PAGE with Coomassie staining (mean of triplicate ± 1 s.d.). (f) DLS characterization of SpyCatcher-mi3 with or without CyRPA-SpyTag conjugation (mean of triplicate ± 1 s.d.).

cells (CyRPA-SpyTag, 42 kDa, 5 disulfide bonds; Pfs25-SpyTag, 21 kDa, 11 disulfide bonds).¹⁸ Conjugation efficiency ranged from 91 to 96% (Figure 3e). Proper assembly of conjugated SpyCatcher-mi3 was validated by DLS. SpyCatcher-mi3 had a hydrodynamic radius of 17.6 ± 4.4 nm before conjugation and 20.9 ± 5.8 nm after conjugation to CyRPA-SpyTag (Figure 3f). Thus, SpyCatcher-mi3 was able to react with high efficiency to a range of antigens, bearing either N- or C-terminally fused SpyTag and produced in eukaryotic or bacterial cells.

For a nanoparticle platform to transition from small-scale laboratory production to clinical and field-settings, it is desirable that the platform is robust and tolerates long-term storage and varying temperature.⁵¹ Inactivation of vaccines through failure of the cold-chain is a major challenge for the cost and efficacy of vaccines in the developing world.^{52,53} In addition, using this modular vaccine assembly strategy, it would be desirable to be able to stockpile the platform, to use in a newly emerging medical or veterinary outbreak challenge.⁵⁴ To test nanoparticle heat stability, purified SpyCatcher-mi3 was incubated in neutral buffer at temperatures ranging from 25 to 95 °C for 1 h. Aggregates were removed by centrifugation, and we measured the proportion of protein in the soluble fraction. Up to 75 °C, at least 80% of the

protein remained in the soluble fraction (Figure 4a). At elevated temperatures a small increase was observed in the hydrodynamic radius, as measured by DLS (Supporting Information, Figure S2b).

Many protein nanoparticles are disrupted by freezing.^{55,56} After four rounds of freeze–thawing, ~15% of SpyCatcher-mi3 was lost to aggregation. However, addition of the common sugar stabilizer trehalose minimized aggregation, resulting in only 3% loss of protein over four rounds (Figure 4b). Beyond the solubility, the SpyCatcher-mi3 particles also remained well-formed after four rounds of freeze–thawing, based on DLS (Figure 4c).

We also evaluated stability to lyophilization. The SpyCatcher-mi3 nanoparticle could be lyophilized and reconstituted without damage to the particle shape, based on DLS (Figure 4d), or to the solubility (Figure 4e). After lyophilization, reconstituted SpyCatcher-mi3 retained good reactivity, as tested by conjugation to SpyTag-MBP (Figure 4f).

For vaccine formulation and to facilitate reaction with antigens which are not soluble themselves at high concentration, it is valuable for the nanoparticles to have high solubility. We found that SpyCatcher-mi3 was highly soluble and could be concentrated to >1 mM (36 mg/mL) (Supporting Information, Figure S2c). This high concentration

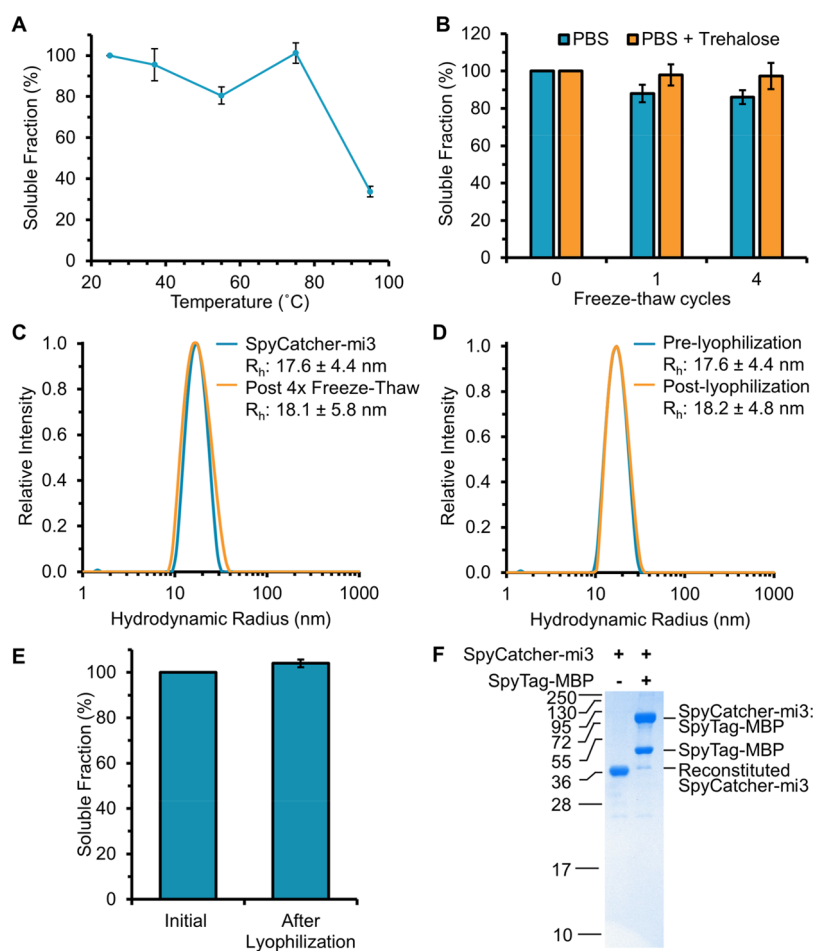


Figure 4. SpyCatcher-mi3 nanoparticles were robust to heating, freezing, and lyophilization. (a) SpyCatcher-mi3 remained soluble after high temperatures. SpyCatcher-mi3 was incubated for 1 h at the indicated temperatures. Samples were centrifuged to remove aggregates, and soluble protein was quantified by densitometry (mean \pm 1 s.d., $n = 3$). (b) SpyCatcher-mi3 remained soluble after freeze–thaw. Soluble protein for SpyCatcher-mi3 was quantified, as in (a), after 1 or 4 cycles of freeze–thawing \pm 1 M trehalose (mean \pm 1 s.d., $n = 3$). (c) Freeze–thaw did not change nanoassembly. DLS of SpyCatcher-mi3 before and after four rounds of freeze–thaw without trehalose. (d) Lyophilization did not change nanoassembly. SpyCatcher-mi3 was analyzed by DLS before lyophilization or after lyophilization and reconstitution in the same volume. (e) SpyCatcher-mi3 soluble fraction, before and after lyophilization with reconstitution in the same buffer volume (mean \pm 1 s.d., $n = 3$). (f) SpyCatcher-mi3 retained reactivity after lyophilization. Reaction of SpyCatcher-mi3 with SpyTag-MBP at 25 °C for 16 h was analyzed by SDS-PAGE with Coomassie staining.

was sustainable following freeze–thaw or storage at 4 °C for 1 week (Supporting Information, Figure S2c).

To streamline modular nanoparticle assembly, it was interesting to explore whether the nanoparticles could conjugate with target proteins without purification of each partner. We added purified SpyTag-mClover3 to *E. coli* cleared lysate expressing SpyCatcher-mi3. mClover3 remains fluorescent in SDS-PAGE, as long as the sample is not boiled before loading. Using fluorescent imaging and Coomassie staining, we saw substantial depletion of the SpyCatcher-mi3 band and formation of a SpyCatcher-mi3:SpyTag-mClover3 conjugate band (Supporting Information, Figure S2d), indicating that nanoparticle decoration can occur without purification.

In considering the mi3 nanoparticle scaffold for vaccine applications, it was important to check for similarity to human sequences, to minimize the chance of activating an auto-immune response. No ortholog of KDPG aldolase exists in humans.⁵⁷ Sequence alignment of mi3 against the human protein database using BLAST revealed no substantial similarity, through coincidence, to any human protein. The top hit was to a 32 amino acid fragment of Interleukin-1

receptor-associated kinase 3 (IRAK3), giving a score of 64, sequence identity 40.6%, and *E*-value: 9.4 (Supporting Information, Figure S3a). *E*-values of 0.1 or greater are generally not considered to be significant.⁵⁸ In comparison, a similar alignment was done for Δ N1-SpyCatcher which is an N-terminally truncated version of SpyCatcher for reduced immunogenicity.⁵⁹ The top hit was a fragment of the Hemicentin-2 human gene that gave a score of 62, sequence identity 29.7%, and *E*-value: 2.8 (Supporting Information, Figure S3b).

Having established good assembly, reactivity, and robustness of the SpyCatcher-mi3 platform, we investigated its immunogenicity. Because of the urgent need to improve malaria vaccination,^{60,61} we focused on immunizing against CyRPA. We validated conjugation of CyRPA-SpyTag to SpyCatcher-mi3 by SDS-PAGE, and free antigen was removed using a high molecular weight cutoff (MWCO) membrane (Figure 5a,b). Mice were injected intramuscularly with 1 μ g total CyRPA for each group. CyRPA-SpyTag alone was compared to the same antigen multimerized using SpyCatcher-mi3 or the previous leading nanoassembly platform for Plug-and-Display Spy-

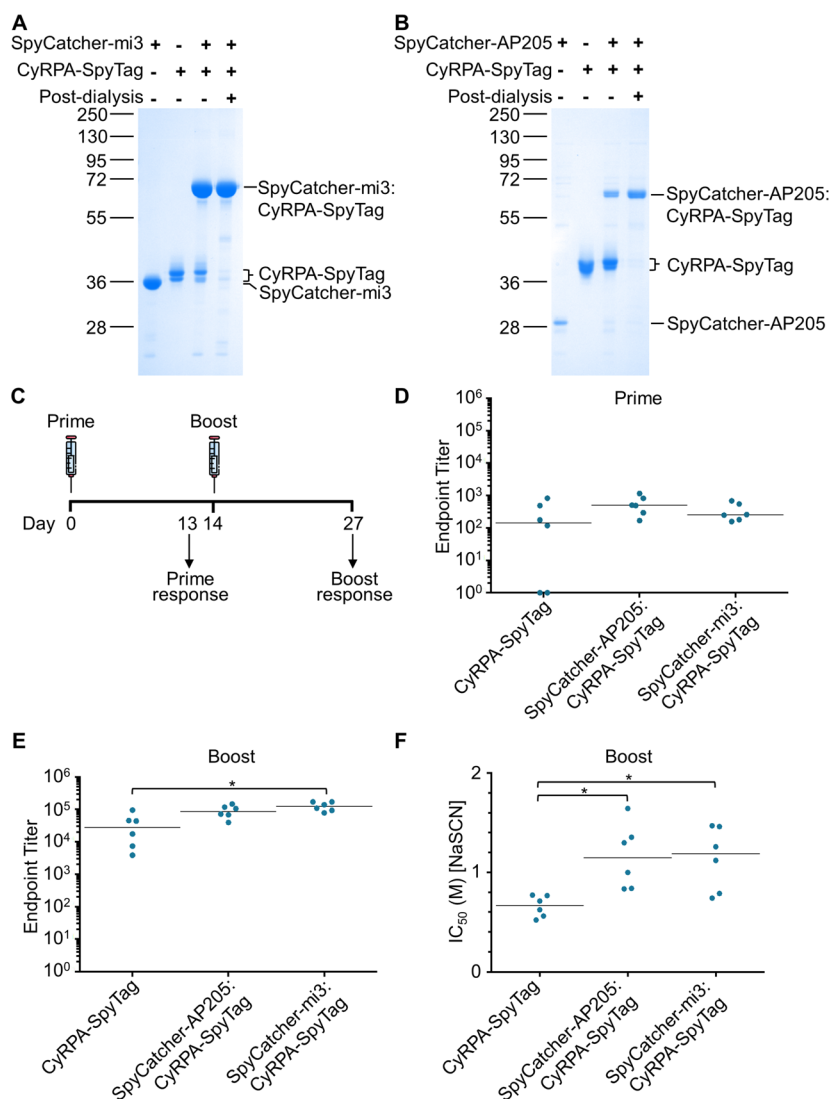


Figure 5. mi3 nanoassembly enhanced immunogenicity. (a) SpyCatcher-mi3 immunogen assembly. SpyCatcher-mi3 was conjugated with CyRPA-SpyTag, and unreacted antigen was removed by dialysis, as analyzed by SDS-PAGE with Coomassie staining. (b) SpyCatcher-AP205 immunogen assembly. SpyCatcher-AP205 was conjugated with CyRPA-SpyTag and analyzed as in (a). (c) Time course of immunization regimen. (d) Antibody titer to CyRPA after the prime. (e) Antibody titer to CyRPA after the boost. (f) Nanoassembly enhanced antibody avidity. The avidity of anti-CyRPA antibodies was assayed, based on resistance to NaSCN-induced dissociation. In each case, the value is plotted for each mouse. The horizontal bar represents the median and a Kruskal–Wallis test followed by Dunn’s multiple comparison post-test was performed. * $p < 0.05$; n.s. $p > 0.05$; $n = 6$.

Catcher-AP205.^{18,34} All immunizations were performed with AddaVax, a potent squalene-oil-in-water emulsion adjuvant based on the MF59 adjuvant that is licensed and used in influenza vaccines.^{62–64} Mice were boosted with the same dosage at 14 days, and antibody titer against CyRPA was measured after prime or postboost *via* enzyme-linked immunosorbent assay (ELISA) (Figure 5c). After priming, 6/6 mice in each group responded to the nanoparticle platforms, while 4/6 responded to the monomeric antigen (Figure 5d). This indicates that there is variability in the immune response to free antigen. However, this difference in titer did not reach significance (Figure 5d).

After boosting, 6/6 mice in each group had an anti-CyRPA antibody response at day 27. There was not a significantly different response comparing SpyCatcher-AP205 multimerization against monomeric antigen (Figure 5e). There was a significantly higher antibody response with SpyCatcher-mi3

assembly compared to monomeric antigen ($p = 0.011$, $n = 6$, Kruskal–Wallis test followed by Dunn’s multiple comparison post-test) (Figure 5e).

The avidity of CyRPA-specific antibodies was analyzed at day 28 (14 days postboost) using a sodium thiocyanate (NaSCN) antibody displacement ELISA.⁶⁵ The molar concentration of NaSCN required to reduce the A_{405} to 50% (IC_{50}) compared to untreated samples was determined. Both SpyCatcher-mi3 and SpyCatcher-AP205 induced CyRPA-specific antibodies with significantly higher avidity compared to CyRPA-SpyTag ($p = 0.028$ for SpyCatcher-mi3; $p = 0.011$ for SpyCatcher-AP205, $n = 6$, Kruskal–Wallis test followed by Dunn’s multiple comparison post-test) (Figure 5f). There was no significant difference in avidity between SpyCatcher-mi3 and SpyCatcher-AP205 (Figure 5f).

CONCLUSION

Nanoparticles must fulfill a stringent series of criteria to be suitable for medical application.^{2,7,8} This work establishes a simple and robust nanoscaffold, suitable for modular multimerization of complex proteins just by mixing. The experiments here also provide insight into nanoparticle features important for high stability and for potent stimulation of an immune response.

Rational modification of a protein computationally designed to assemble into a dodecahedron (i301) enhanced the uniformity of the isolated protein, while increasing both the yield and stability of the resultant nanoparticle. The cysteines mutated in i301 are not accessible for intersubunit disulfide bond formation in the predicted folded structure.³⁹ Therefore, consideration of rare misfolded structures may be important to obtain robust nanoscaffolds.

SpyCatcher-mi3 shows various positive features toward application in vaccine assembly. The platform is robust to freezing, heating, and lyophilization. The high thermoresilience is consistent with the hyperthermophilic origin of the aldolase, suggesting that the mutations to generate i301 and then mi3 did not greatly impair the protein stability. SpyCatcher itself is from a mesophilic organism, *Streptococcus pyogenes*.⁶⁶ However, SpyCatcher has shown the ability to enhance protein thermal resilience in the context of cyclizing enzymes.^{67,68}

For the malaria antigen CyRPA, multimerizing on the SpyCatcher-mi3 scaffold increased the antibody response compared to immunization with monomeric antigen. Analysis of the avidity of the anti-CyRPA specific antibodies also indicated a qualitatively superior response from multimerized antigen. The importance of high avidity antibodies has been emphasized for resisting HIV immune escape^{69,70} and for increasing antibody antiviral effector function.⁷¹ It might be predicted that AP205 would be a more immunogenic nanoscaffold than mi3, having a higher valency (maximum 180 antigens on AP205 versus 60 on mi3)⁷² and efficiently encapsulating RNA, which can stimulate Toll-like receptor (TLR) 7 and 8 signaling.⁷³ Also, AP205 cp3 forms a conventional tightly packed capsid surface, whereas i301 has large pores. In fact, we found comparable antibody titer and avidity from immunization using SpyCatcher-AP205 or SpyCatcher-mi3. Therefore, the more efficient production by *E. coli* may make SpyCatcher-mi3 a more favorable nanoscaffold for future development. A limitation of the SpyCatcher-mi3 platform is that it is important that the protein to be conjugated does not self-associate and thereby promote aggregation. Also, we have not tested the induction of cytotoxic T cell responses using SpyCatcher-mi3, where one would expect viral vectored vaccines to be superior.⁷⁴

The simple production of SpyCatcher-mi3, accessible to any molecular biology laboratory, should facilitate its widespread use by the research community as well as favoring potential clinical development. The lack of sequence homology between SpyCatcher-mi3 and the human genome reduces potential concerns about the platform inducing an autoimmune response. Beyond mi3, there are a number of computationally derived protein nanocages that vary in composition, structure, and cargo packaging.^{75,76} Thus, future work in synthetic nanobiology may establish the factors maximizing nanoparticle immunogenicity, such as the ideal antigen spacing, number, and orientation.^{32,77,78}

METHODS

Cloning. Constructs were cloned using standard PCR methods and Gibson assembly. Inserts were verified by Sanger sequencing. In all cases, the version of SpyCatcher used was Δ N1-SpyCatcher.⁷⁹ The i301 insert³⁹ was synthesized by Genscript. pET28a-SpyCatcher-i301 has the organization: SpyCatcher, (GGG)₄ spacer, i301, GSG spacer, C-tag. pET28a-SpyCatcher-mi3 (GenBank accession no. MH425515 and Addgene plasmid ID 112255) has the same organization, except for mutations C76A and C100A (numbering based on i301 from Hsia *et al.*, Supporting Information Figure S1a)³⁹ introduced by Gibson cloning. pENTR4-LPTOS-CyRPA-SpyTag has the organization: IgG leader of V-kappa sequence, *P. falciparum* CyRPA (3D7), (GSG)₃ spacer, SpyTag, GSG spacer, C-tag (GenBank accession no. MH425516) in the pENTR4-LPTOS backbone.⁸⁰ pENTR4-LPTOS-CyRPA has the organization: IgG leader of V-kappa sequence, CyRPA, GGGS spacer, C-tag. pENTR4-LPTOS-Pfs25-SpyTag for expression in mammalian cells has been previously described (GenBank accession no. KU302811.1).¹⁸ pET28a-SpyTag-MBP⁶⁶ (Addgene plasmid ID 35050), pET28-SpyTag-mClover3,⁸¹ pGEM-SpyCatcher-AP205 cp3,¹⁸ and pET15b-SpyTag-CIDR-(IT4var07)¹⁸ have been previously described.

Expression of SpyCatcher-mi3 Particles. The pET28a expression plasmid of either SpyCatcher-i301 or SpyCatcher-mi3 was transformed into *E. coli* BL21 (DE3)-RIPL (Agilent), and cells were grown for 16 h at 37 °C on LB-Agar plates containing 50 μ g/mL kanamycin. A single colony was picked into a 10 mL starter culture of LB medium containing 50 μ g/mL kanamycin and incubated for 16 h at 37 °C with shaking at 200 rpm. The entire 10 mL culture was then diluted into 1 L LB containing 50 μ g/mL kanamycin and incubated at 37 °C with shaking at 200 rpm. At A₆₀₀ 0.8, cultures were induced with 0.5 mM IPTG and grown for 16–20 h with shaking at 200 rpm at 22 °C.

Purification of SpyCatcher-mi3 Particles. One 500 mL culture-derived pellet was resuspended in 10 mL lysis buffer [25 mM Tris-HCl pH 8.5, 150 mM NaCl, 0.1 mg/mL lysozyme, 1 mg/mL cOmplete mini EDTA-free protease inhibitor (Sigma-Aldrich), 1 mM phenylmethanesulfonyl fluoride (PMSF) (Sigma-Aldrich) at 4 °C] and rotated at 25 °C for 1 h. The lysate was then sonicated on ice for 5 min with rounds of 10 s on and 10 s off, before centrifugation at 16,900 g for 30 min at 4 °C. Capture Select C-tag Affinity Matrix (Thermo Fisher Scientific) (7.5 mL), equilibrated to 25 mM Tris-HCl pH 8.5 with 150 mM NaCl at 4 °C, was added to cleared lysate and incubated on a tube roller at 4 °C for 1 h. The mixture was then added to a polyprep column by gravity filtration and washed with 10 column volumes of 25 mM Tris-HCl pH 8.5 with 150 mM NaCl at 4 °C. Elution buffer (20 mM Tris-HCl pH 7.4 with 2 M MgCl₂ at 4 °C) was added to the column and incubated for 5 min before each elution. Protein in elution was monitored by A₂₈₀. Total eluate was then diluted with a 10 \times stock of 250 mM Tris-HCl pH 8.5 with 1.5 M NaCl at 4 °C, before concentrating in a 20 mL 100 kDa MWCO Vivaspin ultrafiltration unit (Sartorius) and applying to a previously equilibrated HiPrep 16/60 Sephacryl S-400 or S-500 HR (GE Healthcare) on a fast protein liquid chromatography (FPLC) system AKTA Purifier 10 (GE Healthcare). The mobile-phase column buffer was 25 mM Tris-HCl pH 8.5 with 150 mM NaCl, and the applied flow-rate was 1.0 mL/min, all at 4 °C. A high molecular weight gel filtration standard (Bio-Rad, Cat. No. 151–1901) was run on the same column with the same buffer and flow-rate specification. Elution of proteins and standard was monitored at A₂₈₀. The SpyCatcher-mi3 elution in the 65–90 mL range was collected. Collected fractions were concentrated using a 100 kDa spin column, and the concentration was determined using the Pierce bicinchoninic acid (BCA) Assay Kit (Thermo Fisher Scientific).

Expression of SpyCatcher-AP205 VLPs. C41 *E. coli* cells, a kind gift of Anthony Watts (University of Oxford), were transformed with pGEM-SpyCatcher-AP205¹⁸ (GenBank accession number KU302810) and grown for 16 h at 37 °C on an LB-agar plate containing 100 μ g/mL ampicillin. A single colony was picked into a 10 mL starter culture of 2 \times TY medium containing 100 μ g/mL

ampicillin and incubated at 37 °C with shaking at 200 rpm for 16 h. The entire 10 mL culture was then diluted into 1 L 2×TY containing 100 µg/mL ampicillin and incubated at 37 °C with shaking at 200 rpm. At A_{600} of 0.5, cultures were induced with 0.42 mM IPTG and grown for 4–6 h with shaking at 200 rpm at 30 °C. Following the conditions for expression of SpyCatcher-mi3 above decreased the yield of SpyCatcher-AP205.

Purification of SpyCatcher-AP205 VLPs. One 1 L culture-derived pellet was resuspended at 25 °C for 1 h in 10 mL lysis buffer [20 mM Tris-HCl pH 7.8, 150 mM NaCl, 0.1% (v/v) Tween-20, 75 mM imidazole, 0.2 mg/mL lysozyme, 1 mg/mL cOmplete mini EDTA-free protease inhibitor cocktail, 1 mM PMSF, 25 U/mL benzonase]. The lysate was sonicated 4 times for 30 s with a minimum of 1 min between each pulse. The lysate was centrifuged twice at 16,900 g for 45 min at 4 °C. The supernatant was then filtered through a Minisart NML Glass Fiber Filter (1.2 µm pore size) (Sartorius) and then through a Syringe Filter (0.45 µm pore size) (StarLab, cat. no. E4780-1453). The filtrate was incubated with 250 U benzonase (Sigma-Aldrich) for 5 min at 25 °C. One mL of packed Ni-NTA agarose (Qiagen) equilibrated to 75 mM imidazole in buffer [20 mM Tris-HCl pH 7.8, 150 mM NaCl, 0.1% (v/v) Tween-20] was added to the cleared lysate and incubated on a tube roller for 30 min at 4 °C. The resin was then added to a polyprep column by gravity filtration and washed 5 times with 10 column volumes of wash buffer at 4 °C [50 mM Tris-HCl, 150 mM NaCl, 100 mM imidazole, 0.1% (v/v) Tween-20, pH 7.8]. For elution, the polyprep column was capped, 1 mL of elution buffer added [2 M imidazole, 50 mM glycine, 25 mM sodium citrate, 0.1% (v/v) Tween-20, pH 8.5 at 4 °C], the resin incubated for 5 min, and the process repeated until all protein was eluted. Eluate was centrifuged for 30 min at 16,900 g at 4 °C, before transfer to a 300 kDa molecular weight cutoff cellulose ester dialysis tubing (SpectrumLabs) and dialyzed overnight at 4 °C against 1000-fold excess of 50 mM glycine, 25 mM sodium citrate, 0.1% (v/v) Tween-20, pH 8.0, for buffer exchange and depletion of VLP monomer. Dialysis was repeated an additional two times for 3 h. After dialysis, the sample was centrifuged once more at 16,900 g at 4 °C for 30 min to remove any aggregates.

Protein concentration was measured using the BCA assay kit. Protein concentration for nanoparticles refers to the concentration of monomer. The comparison of nanoparticle yield was based upon BCA assays of preps grown and purified on independent days ($n = 3$).

Expression and Purification of Monomeric Proteins. To express CyRPA-SpyTag, suspension Expi293HEK cells (Thermo Fisher Scientific) were cultured in Expi293 Expression media (Thermo Fisher Scientific) with 50 U/mL penicillin/streptomycin (Thermo Fisher Scientific). The cells were grown in a humidified Multitron Cell incubator (Infors HT) at 37 °C with 7% CO₂, rotating at 110–125 rpm. The cells were transiently transfected with either CyRPA-SpyTag or CyRPA using the ExpiFectamine 293 transfection kit (Thermo Fisher Scientific). Cells at a density of 2.5×10^6 cells/mL were transfected with 2.7 µL ExpiFectamine 293 Reagent per 1 µg of plasmid DNA. ExpiFectamine transfection enhancers (Thermo Fisher Scientific) were added 16–18 h post-transfection, and cell supernatant was harvested 4 days post-transfection. Cell supernatants were centrifuged at 218 g to remove residual cells and filtered through 0.45 µm syringe filters, and 1 mg/mL cOmplete mini EDTA-free protease inhibitor cocktail was added. Cell supernatants (40 mL for CyRPA and 240 mL for CyRPA-SpyTag) were added to Capture Select C-tag Affinity Matrix (Thermo Fisher Scientific) and incubated on a tube roller at 4 °C for 1 h. The mixture was then added to a polyprep column by gravity filtration and washed with 10 column volumes of wash buffer (20 mM Tris-HCl, 150 mM NaCl, pH 7.4 at 4 °C). Elution buffer (20 mM Tris-HCl, 2 M MgCl₂, pH 7.4 at 4 °C) was added to the column and incubated for 5 min before each elution. Protein in elution was monitored by A_{280} . Total eluate was concentrated in a 20 mL 10 kDa MWCO Vivaspın ultrafiltration unit (Sartorius) and applied to a previously equilibrated HiLoad 16/600 Superdex 200 pg column (GE Healthcare) on an AKTA Purifier 10. The mobile-phase buffer was either 50 mM Tris-HCl, 150 mM NaCl pH 7.4 (CyRPA-SpyTag) or 50 mM Tris-borate pH 7.25

(CyRPA), and the applied flow-rate was 1.0 mL/min all at 4 °C. Elution of proteins was monitored by A_{280} . Elutions were collected in the 74–97 mL range for CyRPA-SpyTag and in the 60–72 mL range for CyRPA.

SpyTag-MBP and SpyTag-CIDR were expressed in *E. coli* as described.¹⁸ SpyTag-mClover3 was also expressed in *E. coli* as described.⁸¹

Reactions. SpyCatcher-mi3 at 10 µM was reacted with 3× molar excess of CyRPA-SpyTag, SpyTag-CIDR, SpyTag-MBP, or Pfs25-SpyTag for 16 h at 25 °C in 25 mM Tris-HCl, 150 mM NaCl, pH 8.5 at 4 °C. Coupling efficiency was analyzed by SDS-PAGE with Coomassie staining.

Dynamic Light Scattering (DLS). Protein samples were centrifuged for 30 min at 16,900 g at 4 °C to remove any aggregates, and 20 µL was loaded into a reusable cuvette. Proteins were diluted in their native buffer to a suitable concentration enabling stable measurement. The buffer used to dilute samples was also centrifuged for 30 min at 16,900 g before use. Each protein sample was measured at 20 °C using an Omnisizer (Viscotek) with 10 scans of 10 s each. The intensity distribution from the scans was plotted, and the mean and standard deviation calculated in Excel. To compare aggregation after long-term storage, SpyCatcher-mi3 and SpyCatcher-i301 samples at 30 µM in 25 mM Tris-HCl, 150 mM NaCl, pH 8.5 were sterile-filtered and stored in Parafilm-wrapped microcentrifuge tubes at 4 °C for 5 weeks, before processing as above.

Transmission Electron Microscopy (TEM). SpyCatcher-mi3 nanoparticles (0.2 mg/mL) were applied to freshly glow-discharged carbon 200 mesh copper grids for 2 min and blotted with filter paper. Samples were stained with 2% uranyl acetate for 10 s and then blotted and air-dried. Grids were imaged in a FEI Tecnai T12 transmission electron microscope at 120 kV using a Gatan US1000 CCD camera. Using FIJI (ImageJ) and the Analyze-Measure tool, particle diameter was measured ($n = 100$). Measurements were plotted with 2 nm bin size, and the mean and standard deviation were calculated in Excel.

Sequence Alignment. Amino acid sequences of mi3 and Δ N1-SpyCatcher were entered into UniProt BLAST and aligned against all proteins in the human protein database (UniProtKB_human) with the default settings (*E*-threshold: 10, matrix: auto, filtering: none).⁸² The top match was aligned and examined for expect (*E*)-value. *E*-values relate to the number of hits expected by chance when searching a database of that size. *E*-values >0.1 are considered not significant.⁵⁸ A position-specific scoring matrix based on conservation for the amino acid sequence of *T. maritima* KDPG aldolase was generated using PSI-BLAST with three iterations, and representative sequences from different bacteria are shown.⁸³

SDS-PAGE and Reaction Quantification. SDS-PAGE was performed with 12 or 18% Tris-glycine gels using an XCell SureLock system (Thermo Fisher Scientific). Protein samples were loaded with 6× SDS-PAGE loading buffer [0.23 M Tris-HCl pH 6.8, 24% (v/v) glycerol, 120 µM bromophenol blue, 0.23 M SDS] and heated for 3 min at 99 °C before loading on the gel. On reduced samples, loading buffer contained 170 µM 2-mercaptoethanol. SDS-PAGE was performed at 200 V in 25 mM Tris-HCl and 192 mM glycine, 0.1% (w/v) SDS, pH 8.5. Gels were stained with InstantBlue Coomassie stain (Expedeon), destained using Milli-Q water, and imaged using ChemiDoc XRS imager and ImageLab (version 5.2) software (BioRad). ImageLab was also used for band quantification. To assess the percentage of SpyCatcher-mi3 particle that had reacted with antigen, a sample of unreacted SpyCatcher-mi3 at the same starting concentration was run on the gel and defined as 100% unreacted. % Conjugation was defined as $100 \times [1 - (\text{SpyCatcher-mi3 band after antigen incubation}) / (\text{SpyCatcher-mi3 band in the absence of antigen})]$.

Temperature-Dependent Solubility Assay. Thirty µL SpyCatcher-mi3 at 30 µM in 25 mM Tris-HCl, 150 mM NaCl, pH 8.5 was incubated at 25, 37, 55, 75, or 95 °C for 1 h and then cooled to 4 °C for 10 min on a C1000 thermal cycler (Bio-Rad). Following heating, aggregated proteins were pelleted by centrifugation at 16,900 g for 30 min at 4 °C. The supernatant was run on SDS-PAGE and analyzed by densitometry. The sample held at 25 °C was defined as

100% soluble. All samples were run in triplicate (plotted as mean \pm 1 s.d.). Samples were adjusted to 0.125 mg/mL, before analyzing by DLS as above.

Freeze–Thaw Stability Assay. 180 μ L SpyCatcher-mi3 at 20 μ M in PBS (137 mM NaCl, 2.7 mM KCl, 10 mM Na₂HPO₄, 1.8 mM KH₂PO₄, pH 7.4 at 4 °C) with or without 1 M trehalose (Sigma-Aldrich) was analyzed by SDS-PAGE and DLS, either at the initial time point or after 1 or 4 cycles of freeze–thaw. Each cycle of freeze–thaw consisted of placing the sample in a thin-wall PCR tube (StarLab) for 20 min into a –80 °C freezer, followed by 15 min in an Eppendorf ThermoMixer C at 25 °C. Each sample was spun at 16,900 g for 30 min at 4 °C to remove aggregates, before the supernatant was assayed by SDS-PAGE with Coomassie staining or DLS. The sample without freeze–thaw was defined as 100% soluble.

Lyophilization Stability Assay. A 100 μ L aliquot of SpyCatcher-mi3 particles at 10 μ M in 25 mM Tris-HCl, 150 mM NaCl, pH 8.5 at 4 °C was prepared in a 100 μ L thin-wall PCR tube. Samples were snap-frozen in a dry ice-ethanol bath for 30 min. A BenchTop 2K freeze-dryer (VirTis) was used for 24 h at 0.14 mbar and –72.5 °C. Lyophilized sample was reconstituted in the same volume of Milli-Q water and centrifuged at 16,900 g for 30 min to remove any aggregates, before analysis of the supernatant by SDS-PAGE with Coomassie staining or DLS. To test reactivity of SpyCatcher-mi3 after lyophilization, 5 μ M SpyCatcher-mi3 was reacted with 15 μ M SpyTag-MBP for 16 h at 25 °C, before analysis by SDS-PAGE with Coomassie staining.

Concentration Stability Assay. SpyCatcher-mi3 in 25 mM Tris-HCl, 150 mM NaCl, pH 8.5 at 4 °C was concentrated in a 500 μ L 300 kDa MWCO Vivaspine ultrafiltration unit (Sartorius) to a final concentration of 1090 μ M. Concentrated protein sample was then either stored at 4 °C or underwent one round of freeze–thaw (following the procedure in the Freeze–Thaw Stability Assay section). The samples were then centrifuged for 30 min at 16,900 g at 4 °C, before the protein concentration in the supernatant was measured by BCA assay on triplicate samples.

Preparation of Immunogens. SpyCatcher-mi3 nanoparticles (10 μ M) with 3 \times molar excess of CyRPA-SpyTag or SpyCatcher-AP205 VLPs with 1.5 \times molar excess of CyRPA-SpyTag were incubated for 16–18 h at 25 °C in PBS. The reaction was then dialyzed 4 times in a 300 kDa MWCO cellulose ester dialysis tubing against a 4000-fold excess of PBS with 0.1% (v/v) Tween-20 to remove unreacted CyRPA-SpyTag. Conjugation of CyRPA-SpyTag to SpyCatcher-mi3 or SpyCatcher-AP205 was validated by SDS-PAGE with Coomassie staining. Reducing conditions were employed for SpyCatcher-AP205 analysis *via* SDS-PAGE because of the AP205 intersubunit disulfide bonds. Endotoxin was removed from each reaction using Triton X-114 phase separation.⁸⁴ The reaction volume was transferred to 1.5 mL endotoxin-free microcentrifuge tubes (StarLab, cat. no. E1415–1510), and 1% (v/v) Triton X-114 was added to each sample. Samples were then incubated on ice until all Triton X-114 was dissolved, followed by another 5 min incubation on ice. Samples were then incubated at 37 °C for 5 min and centrifuged for 1 min at 16,900 g at 37 °C. The supernatant was pipetted off, and the entire procedure repeated two times. Endotoxin concentration was determined using the Limulus amoebocyte lysate (LAL) Chromogenic Endotoxin Quantitation Kit (Thermo Fisher Scientific) according to the manufacturer's instructions. For all vaccines, endotoxin level was below 1 endotoxin unit/mL. Vaccine doses were matched to 1 μ g CyRPA equivalent for each group and diluted with sterile endotoxin-free PBS with 0.1% (v/v) Tween-20 to a final volume of 25 μ L per dose. Each vaccine batch was prepared within 5 days of immunization and kept at 4 °C.

Immunizations. All animal experiments and procedures were performed according to the UK Animals (Scientific Procedures) Act Project License (PPL PA7D20B85) and approved by the University of Oxford Animal Welfare and Ethical Review Body. Age-matched female BALB/c mice (Envigo), housed in a specific-pathogen free environment, were immunized with equal amounts of vaccines intramuscularly into each leg. Immunizations were performed as a prime-boost regimen (prime on day 0, boost on day 14). The vaccines

were prepared in 0.22 μ m syringe filter-sterilized endotoxin-free PBS with 0.1% Tween-20 and formulated 1:1 in the adjuvant AddaVax (InvivoGen) (25 μ L/per dose). The protein immunogen and the AddaVax adjuvant were mixed together by pipetting. Blood samples were harvested on days 13 and 27 to obtain sera for analysis of end point ELISA titers and on day 28 for antibody avidity ELISA. Blood samples were left to clot overnight at 4 °C, and sera were transferred to fresh microcentrifuge tubes after 10 min centrifugation at 8600 g in a benchtop centrifuge. Six mice were used for each condition.

End Point ELISA. MaxiSorp plates (Thermo Fisher Scientific) were coated overnight at 4 °C with CyRPA at 1 μ g/mL in coating buffer (15 mM sodium carbonate with 35 mM sodium bicarbonate, pH 9.6). Plates were washed six times with PBS/T (PBS with 0.5% Tween-20) and blocked with PBS/T with 10% skim milk for 1 h at 25 °C. Plates were washed six times with PBS/T and incubated with duplicates of 3-fold serially diluted serum samples for 2 h at 25 °C. Following a wash step with PBS/T, goat antimouse total IgG conjugated to alkaline phosphatase (Sigma-Aldrich) (1:3,000 dilution in PBS/T) was added to the plates, and the plates were incubated for 1 h at 25 °C. After a final wash step with PBS/T, *p*-nitrophenylphosphate (Sigma-Aldrich) (1 mg/mL) diluted in 1 M diethanolamine, pH 9.8 (Thermo Scientific) was used as a developing substrate. A₄₀₅ was obtained using a SpectraMAX M3 plate reader (Molecular 322 Devices). The end point titer is defined as the *x*-axis intercept of the dilution curve at an absorbance value greater than the mean A₄₀₅ plus three standard deviations for a serum sample from a naïve mouse at a serum dilution of 1:100.

Antibody Avidity ELISA. Antibody avidity was assessed at day 28 using a sodium thiocyanate (NaSCN) displacement ELISA. MaxiSorp plates (Thermo Fisher Scientific) were coated with CyRPA overnight at 4 °C and blocked and washed with PBS/T as described above. Serum samples were individually diluted to reach an A₄₀₅ of approximately 1.5 and plated in duplicate. Three of the samples from the CyRPA-SpyTag immunized group were analyzed at their maximum reachable A₄₀₅ at 0.4, 0.5, and 0.9. Following 2 h incubation at 25 °C and washing with PBS/T, the indicated concentration of NaSCN (0–7 M) was added to the wells. The plates were incubated for 15 min at 25 °C, followed by washing with PBS/T, and then incubation with secondary antibody and substrate as above. The intercept at which the molar concentration of NaSCN had reduced the A₄₀₅ to 50% for individual samples was used to give IC₅₀.

Statistical Analysis of Immunizations. Statistical analysis was performed using GraphPad Prism 7.0d. Comparisons were made using a Kruskal–Wallis test. Dunn's multiple comparison post-test was performed for significant values. The *p* values above 0.05 were reported as nonsignificant (n.s.).

Further information and request for resources and reagents should be directed to and will be fulfilled by the lead contact, Mark Howarth (mark.howarth@bioch.ox.ac.uk).

ASSOCIATED CONTENT

Supporting Information

The Supporting Information is available free of charge on the ACS Publications website at DOI: [10.1021/acsnano.8b02805](https://doi.org/10.1021/acsnano.8b02805).

Sequence alignment of *Thermotoga maritima* KDPG aldolase, i301, and mi3 and conservation of aldolase sequence; time-course of SpyCatcher-mi3 reactivity, heat stability determined by DLS, stability at high concentration and reactivity in cleared lysate; sequence similarity of mi3 and SpyCatcher to the human genome (PDF)

AUTHOR INFORMATION

Corresponding Author

*E-mail: mark.howarth@bioch.ox.ac.uk.

ORCID

Mark Howarth: 0000-0001-8870-7147

Author Contributions

[§]These authors contributed equally. T.U.J.B. and A.C.A. performed all experiments. T.U.J.B., A.C.A., S.J.D., and M.H. designed the experiments. T.U.J.B., A.C.A., and M.H. wrote the paper. All authors analyzed the data.

Notes

The authors declare the following competing financial interest(s): M.H. is an inventor on a patent regarding peptide targeting *via* spontaneous amide bond formation (EP2534484). M.H. and S.J.D. are SpyBiotech shareholders and consultants.

ACKNOWLEDGMENTS

Funding for T.U.J.B. was provided by the Clarendon Scholarship and St. Edmund Hall, Oxford. Funding for A.C.A., S.J.D., and M.H. was from the Medical Research Council (MR/P001351/1). S.J.D. is also a Jenner Investigator, a Lister Institute Research Prize Fellow, and a Wellcome Trust Senior Fellow (106917/Z/15/Z). We gratefully acknowledge Errin Johnson (Bioimaging Facility, Sir William Dunn School of Pathology, University of Oxford) for assistance with TEM, David Pattinson for assistance with malaria immunology (Jenner Institute, University of Oxford), and Matteo Ferla (Department of Biochemistry, University of Oxford) for assistance with bioinformatics.

REFERENCES

- (1) Kiessling, L. L.; Gestwicki, J. E.; Strong, L. E. Synthetic Multivalent Ligands as Probes of Signal Transduction. *Angew. Chem., Int. Ed.* **2006**, *45*, 2348–2368.
- (2) Mitragotri, S.; Anderson, D. G.; Chen, X.; Chow, E. K.; Ho, D.; Kabanov, A. V.; Karp, J. M.; Kataoka, K.; Mirkin, C. A.; Petrosko, S. H.; Shi, J.; Stevens, M. M.; Sun, S.; Teoh, S.; Venkatraman, S. S.; Xia, Y.; Wang, S.; Gu, Z.; Xu, C. Accelerating the Translation of Nanomaterials in Biomedicine. *ACS Nano* **2015**, *9*, 6644–6654.
- (3) Zhang, W.-B.; Sun, F.; Tirrell, D. A.; Arnold, F. H. Controlling Macromolecular Topology with Genetically Encoded SpyTag-SpyCatcher Chemistry. *J. Am. Chem. Soc.* **2013**, *135*, 13988–13997.
- (4) Polka, J. K.; Hays, S. G.; Silver, P. A. Building Spatial Synthetic Biology with Compartments, Scaffolds, and Communities. *Cold Spring Harbor Perspect. Biol.* **2016**, *8*, a024018.
- (5) Uchida, M.; McCoy, K.; Fukuto, M.; Yang, L.; Yoshimura, H.; Miettinen, H. M.; LaFrance, B.; Patterson, D. P.; Schwarz, B.; Karty, J. A.; Prevelige, P. E.; Lee, B.; Douglas, T. Modular Self-Assembly of Protein Cage Lattices for Multistep Catalysis. *ACS Nano* **2018**, *12*, 942–953.
- (6) Wilhelm, S.; Tavares, A. J.; Dai, Q.; Ohta, S.; Audet, J.; Dvorak, H. F.; Chan, W. C. W. Analysis of Nanoparticle Delivery to Tumours. *Nat. Rev. Mater.* **2016**, *1*, 16014.
- (7) Shi, J.; Kantoff, P. W.; Wooster, R.; Farokhzad, O. C. Cancer Nanomedicine: Progress, Challenges and Opportunities. *Nat. Rev. Cancer* **2017**, *17*, 20–37.
- (8) Effio, C. L.; Hubbuch, J. Next Generation Vaccines and Vectors: Designing Downstream Processes for Recombinant Protein-Based Virus-like Particles. *Biotechnol. J.* **2015**, *10*, 715–727.
- (9) Nestola, P.; Peixoto, C.; Silva, R. R. J. S.; Alves, P. M.; Mota, J. P. B.; Carrondo, M. J. T. Improved Virus Purification Processes for Vaccines and Gene Therapy. *Biotechnol. Bioeng.* **2015**, *112*, 843–857.
- (10) Jennings, G. T.; Bachmann, M. F. The Coming of Age of Virus-like Particle Vaccines. *Biol. Chem.* **2008**, *389*, 521–536.
- (11) Mohsen, M. O.; Zha, L.; Cabral-Miranda, G.; Bachmann, M. F. Major Findings and Recent Advances in Virus-like Particle (VLP)-Based Vaccines. *Semin. Immunol.* **2017**, *34*, 123–132.
- (12) Charleston, B.; Graham, S. P. Recent Advances in Veterinary Applications of Structural Vaccinology. *Curr. Opin. Virol.* **2018**, *29*, 33–38.
- (13) Kraan, H.; van der Stel, W.; Kersten, G.; Amorij, J.-P. Alternative Administration Routes and Delivery Technologies for Polio Vaccines. *Expert Rev. Vaccines* **2016**, *15*, 1029–1040.
- (14) Berlanda Scorza, F.; Tsvetnitsky, V.; Donnelly, J. J. Universal Influenza Vaccines: Shifting to Better Vaccines. *Vaccine* **2016**, *34*, 2926–2933.
- (15) Silva, J. V. J.; Lopes, T. R. R.; de Oliveira-Filho, E. F.; Oliveira, R. A. S.; Durães-Carvalho, R.; Gil, L. H. V. G. Current Status, Challenges and Perspectives in the Development of Vaccines against Yellow Fever, Dengue, Zika and Chikungunya Viruses. *Acta Trop.* **2018**, *182*, 257–263.
- (16) Huang, D. B.; Wu, J. J.; Tyring, S. K. A Review of Licensed Viral Vaccines, Some of Their Safety Concerns, and the Advances in the Development of Investigational Viral Vaccines. *J. Infect.* **2004**, *49*, 179–209.
- (17) Li, Y.; Leneghan, D. B.; Miura, K.; Nikolaeva, D.; Brian, I. J.; Dicks, M. D. J.; Fyfe, A. J.; Zakutansky, S. E.; de Cassan, S.; Long, C. A.; Draper, S. J.; Hill, A. V. S.; Hill, F.; Biswas, S. Enhancing Immunogenicity and Transmission-Blocking Activity of Malaria Vaccines by Fusing Pfs25 to IMX313 Multimerization Technology. *Sci. Rep.* **2016**, *6*, 18848.
- (18) Brune, K. D.; Leneghan, D. B.; Brian, I. J.; Ishizuka, A. S.; Bachmann, M. F.; Draper, S. J.; Biswas, S.; Howarth, M. Plug-and-Display: Decoration of Virus-Like Particles *via* Isopeptide Bonds for Modular Immunization. *Sci. Rep.* **2016**, *6*, 19234.
- (19) Poteet, E.; Lewis, P.; Chen, C.; Ho, S. O.; Do, T.; Chiang, S.; Labranche, C.; Montefiori, D.; Fujii, G.; Yao, Q. Toll-like Receptor 3 Adjuvant in Combination with Virus-like Particles Elicit a Humoral Response against HIV. *Vaccine* **2016**, *34*, 5886–5894.
- (20) Brune, K. D.; Buldun, C. M.; Li, Y.; Taylor, I. J.; Brod, F.; Biswas, S.; Howarth, M. Dual Plug-and-Display Synthetic Assembly Using Orthogonal Reactive Proteins for Twin Antigen Immunization. *Bioconjugate Chem.* **2017**, *28*, 1544–1551.
- (21) Bachmann, M. F.; Jennings, G. T. Vaccine Delivery: A Matter of Size, Geometry, Kinetics and Molecular Patterns. *Nat. Rev. Immunol.* **2010**, *10*, 787–796.
- (22) Schiller, J.; Lowy, D. Explanations for the High Potency of HPV Prophylactic Vaccines. *Vaccine* **2018**, *36*, 4768.
- (23) Jegerlehner, A.; Storni, T.; Lipowsky, G.; Schmid, M.; Pumpens, P.; Bachmann, M. F. Regulation of IgG Antibody Responses by Epitope Density and CD21-Mediated Costimulation. *Eur. J. Immunol.* **2002**, *32*, 3305–3314.
- (24) Bachmann, M. F.; Rohrer, U. H.; Kündig, T. M.; Bürki, K.; Hengartner, H.; Zinkernagel, R. M. The Influence of Antigen Organization on B Cell Responsiveness. *Science* **1993**, *262*, 1448–1451.
- (25) Gomes, A.; Mohsen, M.; Bachmann, M. Harnessing Nanoparticles for Immunomodulation and Vaccines. *Vaccines* **2017**, *5*, 6.
- (26) Charlton Hume, H. K.; Lua, L. H. L. Platform Technologies for Modern Vaccine Manufacturing. *Vaccine* **2017**, *35*, 4480–4485.
- (27) Walker, A.; Skamel, C.; Nassal, M. SplitCore: An Exceptionally Versatile Viral Nanoparticle for Native Whole Protein Display Regardless of 3D Structure. *Sci. Rep.* **2011**, *1*, 5.
- (28) Patel, K. G.; Swartz, J. R. Surface Functionalization of Virus-Like Particles by Direct Conjugation Using Azide–Alkyne Click Chemistry. *Bioconjugate Chem.* **2011**, *22*, 376–387.
- (29) Billaud, J.-N.; Peterson, D.; Barr, M.; Chen, A.; Sallberg, M.; Garduno, F.; Goldstein, P.; McDowell, W.; Hughes, J.; Jones, J.; Milich, D. Combinatorial Approach to Hepadnavirus-like Particle Vaccine Design. *J. Virol.* **2005**, *79*, 13656–13666.
- (30) Caldeira, J. C.; Peabody, D. S. Thermal Stability of RNA Phage Virus-like Particles Displaying Foreign Peptides. *J. Nanobiotechnol.* **2011**, *9*, 22.
- (31) Janssens, M. E.; Geysen, D.; Broos, K.; De Goeyse, I.; Robbens, J.; Van Petegem, F.; Timmermans, J.-P.; Guisez, Y. Folding Properties of the Hepatitis B Core as a Carrier Protein for Vaccination Research. *Amino Acids* **2010**, *38*, 1617–1626.
- (32) Leneghan, D. B.; Miura, K.; Taylor, I. J.; Li, Y.; Jin, J.; Brune, K. D.; Bachmann, M. F.; Howarth, M.; Long, C. A.; Biswas, S.

- Nanoassembly Routes Stimulate Conflicting Antibody Quantity and Quality for Transmission-Blocking Malaria Vaccines. *Sci. Rep.* **2017**, *7*, 3811.
- (33) Nunes, S. F.; Hamers, C.; Ratinier, M.; Shaw, A.; Brunet, S.; Hudelet, P.; Palmarini, M. A Synthetic Biology Approach for a Vaccine Platform against Known and Newly Emerging Serotypes of Bluetongue Virus. *J. Virol.* **2014**, *88*, 12222–12232.
- (34) Thrane, S.; Janitzek, C. M.; Matondo, S.; Resende, M.; Gustavsson, T.; de Jongh, W. A.; Clemmensen, S.; Roeffen, W.; van de Vegte-Bolmer, M.; van Gemert, G. J.; Sauerwein, R.; Schiller, J. T.; Nielsen, M. A.; Theander, T. G.; Salanti, A.; Sander, A. F. Bacterial Superglue Enables Easy Development of Efficient Virus-like Particle Based Vaccines. *J. Nanobiotechnol.* **2016**, *14*, 30.
- (35) Palladini, A.; Thrane, S.; Janitzek, C. M.; Pihl, J.; Clemmensen, S. B.; de Jongh, W. A.; Clausen, T. M.; Nicoletti, G.; Landuzzi, L.; Penichet, M. L.; Balboni, T.; Ianzano, M. L.; Giusti, V.; Theander, T. G.; Nielsen, M. A.; Salanti, A.; Lollini, P. L.; Nanni, P.; Sander, A. F. Virus-like Particle Display of HER2 Induces Potent Anti-Cancer Responses. *Oncoimmunology* **2018**, *7*, e1408749.
- (36) Frank, S.; Lawrence, A. D.; Prentice, M. B.; Warren, M. J. Bacterial Microcompartments Moving into a Synthetic Biological World. *J. Biotechnol.* **2013**, *163*, 273–279.
- (37) Sutter, M.; Greber, B.; Aussignargues, C.; Kerfeld, C. A. Assembly Principles and Structure of a 6.5-MDa Bacterial Microcompartment Shell. *Science* **2017**, *356*, 1293–1297.
- (38) Rother, M.; Nussbaumer, M. G.; Renggli, K.; Bruns, N. Protein Cages and Synthetic Polymers: A Fruitful Symbiosis for Drug Delivery Applications, Bionanotechnology and Materials Science. *Chem. Soc. Rev.* **2016**, *45*, 6213–6249.
- (39) Hsia, Y.; Bale, J. B.; Gonen, S.; Shi, D.; Sheffler, W.; Fong, K. K.; Nattermann, U.; Xu, C.; Huang, P.-S.; Ravichandran, R.; Yi, S.; Davis, T. N.; Gonen, T.; King, N. P.; Baker, D. Design of a Hyperstable 60-Subunit Protein Icosahedron. *Nature* **2016**, *535*, 136–139.
- (40) Jin, J.; Hjerrild, K. A.; Silk, S. E.; Brown, R. E.; Labbé, G. M.; Marshall, J. M.; Wright, K. E.; Bezemer, S.; Clemmensen, S. B.; Biswas, S.; Li, Y.; El-Turabi, A.; Douglas, A. D.; Hermans, P.; Detmers, F. J.; de Jongh, W. A.; Higgins, M. K.; Ashfield, R.; Draper, S. J. Accelerating the Clinical Development of Protein-Based Vaccines for Malaria by Efficient Purification Using a Four Amino Acid C-Terminal “C-Tag”. *Int. J. Parasitol.* **2017**, *47*, 435–446.
- (41) Gaberc-Porekar, V.; Menart, V. Perspectives of Immobilized-Metal Affinity Chromatography. *J. Biochem. Biophys. Methods* **2001**, *49*, 335–360.
- (42) Jacobsen, M. T.; Fairhead, M.; Fogelstrand, P.; Howarth, M. Amine Landscaping to Maximize Protein-Dye Fluorescence and Ultrastable Protein-Ligand Interaction. *Cell Chem. Biol.* **2017**, *24*, 1040–1047.
- (43) Fierer, J. O.; Veggiani, G.; Howarth, M. SpyLigase Peptide-Peptide Ligation Polymerizes Affibodies to Enhance Magnetic Cancer Cell Capture. *Proc. Natl. Acad. Sci. U. S. A.* **2014**, *111*, E1176–E1181.
- (44) Chen, Y.; Liu, Y.; Zhang, G.; Wang, A.; Dong, Z.; Qi, Y.; Wang, J.; Zhao, B.; Li, N.; Jiang, M. Human Papillomavirus L1 Protein Expressed in *Escherichia Coli* Self-Assembles into Virus-like Particles That Are Highly Immunogenic. *Virus Res.* **2016**, *220*, 97–103.
- (45) Veggiani, G.; Zakeri, B.; Howarth, M. Superglue from Bacteria: Unbreakable Bridges for Protein Nanotechnology. *Trends Biotechnol.* **2014**, *32*, 506–512.
- (46) Lau, C. K. Y.; Turner, L.; Jespersen, J. S.; Lowe, E. D.; Petersen, B.; Wang, C. W.; Petersen, J. E. V.; Lusingu, J.; Theander, T. G.; Lavstsen, T.; Higgins, M. K. Structural Conservation despite Huge Sequence Diversity Allows EPCR Binding by the PfEMP1 Family Implicated in Severe Childhood Malaria. *Cell Host Microbe* **2015**, *17*, 118–129.
- (47) Sala, K. A.; Angrisano, F.; Da, D. F.; Taylor, I. J.; Churcher, T. S.; Blagborough, A. M. Immunization with Transgenic Rodent Malaria Parasites Expressing Pfs25 Induces Potent Transmission-Blocking Activity. *Sci. Rep.* **2018**, *8*, 1573.
- (48) Nikolaeva, D.; Draper, S. J.; Biswas, S. Toward the Development of Effective Transmission-Blocking Vaccines for Malaria. *Expert Rev. Vaccines* **2015**, *14*, 653–680.
- (49) Dreyer, A. M.; Matile, H.; Papastogiannidis, P.; Kamber, J.; Favuzza, P.; Voss, T. S.; Wittlin, S.; Pluschke, G. Passive Immunoprotection of *Plasmodium Falciparum*-Infected Mice Designates the CyRPA as Candidate Malaria Vaccine Antigen. *J. Immunol.* **2012**, *188*, 6225–6237.
- (50) França, C. T.; White, M. T.; He, W. Q.; Hostetler, J. B.; Brewster, J.; Frato, G.; Malhotra, I.; Gruszczyk, J.; Huon, C.; Lin, E.; Kiniboro, B.; Yadava, A.; Siba, P.; Galinski, M. R.; Healer, J.; Chitnis, C.; Cowman, A. F.; Takashima, E.; Tsuboi, T.; Tham, W. H.; et al. Identification of Highly-Protective Combinations of *Plasmodium Vivax* Recombinant Proteins for Vaccine Development. *eLife* **2017**, *6*, e28673.
- (51) Jain, N. K.; Sahni, N.; Kumru, O. S.; Joshi, S. B.; Volkin, D. B.; Russell Middaugh, C. Formulation and Stabilization of Recombinant Protein Based Virus-like Particle Vaccines. *Adv. Drug Delivery Rev.* **2015**, *93*, 42–55.
- (52) Kumru, O. S.; Joshi, S. B.; Smith, D. E.; Middaugh, C. R.; Prusik, T.; Volkin, D. B. Vaccine Instability in the Cold Chain: Mechanisms, Analysis and Formulation Strategies. *Biologicals* **2014**, *42*, 237–259.
- (53) Hanson, C. M.; George, A. M.; Sawadogo, A.; Schreiber, B. Is Freezing in the Vaccine Cold Chain an Ongoing Issue? A Literature Review. *Vaccine* **2017**, *35*, 2127–2133.
- (54) Preiss, S.; Garçon, N.; Cunningham, A. L.; Strugnell, R.; Friedland, L. R. Vaccine Provision: Delivering Sustained & Widespread Use. *Vaccine* **2016**, *34*, 6665–6671.
- (55) Devignot, S.; Bergeron, E.; Nichol, S.; Mirazimi, A.; Weber, F. A Virus-like Particle System Identifies the Endonuclease Domain of Crimean-Congo Hemorrhagic Fever Virus. *J. Virol.* **2015**, *89*, 5957–5967.
- (56) Chen, D.; Tyagi, A.; Carpenter, J.; Perkins, S.; Sylvester, D.; Guy, M.; Kristensen, D. D.; Braun, L. T. J. Characterization of the Freeze Sensitivity of a Hepatitis B Vaccine. *Hum. Vaccines* **2009**, *5*, 26–32.
- (57) Bell, B. J.; Watanabe, L.; Rios-Steiner, J. L.; Tulinsky, A.; Lebiada, L.; Arni, R. K. Structure of 2-Keto-3-Deoxy-6-Phosphoglucuronate (KDPG) Aldolase from *Pseudomonas Putida*. *Acta Crystallogr., Sect. D: Biol. Crystallogr.* **2003**, *59*, 1454–1458.
- (58) Pearson, W. R. An Introduction to Sequence Similarity (“homology”) Searching. *Curr. Protoc. Bioinforma.* **2013**, *42*, 3.1.1–3.1.8.
- (59) Liu, Z.; Zhou, H.; Wang, W.; Tan, W.; Fu, Y.-X.; Zhu, M. A Novel Method for Synthetic Vaccine Construction Based on Protein Assembly. *Sci. Rep.* **2015**, *4*, 7266.
- (60) Rabinovich, R. N.; Drakeley, C.; Djimde, A. A.; Hall, B. F.; Hay, S. I.; Hemingway, J.; Kaslow, D. C.; Noor, A.; Okumu, F.; Steketee, R.; Tanner, M.; Wells, T. N. C.; Whittaker, M. A.; Winzeler, E. A.; Wirth, D. F.; Whitfield, K.; Alonso, P. L. MalERA: An Updated Research Agenda for Malaria Elimination and Eradication. *PLoS Med.* **2017**, *14*, e1002456.
- (61) Healer, J.; Cowman, A. F.; Kaslow, D. C.; Birkett, A. J. Vaccines to Accelerate Malaria Elimination and Eventual Eradication. *Cold Spring Harbor Perspect. Med.* **2017**, *7*, a025627.
- (62) Alving, C. R.; Peachman, K. K.; Rao, M.; Reed, S. G. Adjuvants for Human Vaccines. *Curr. Opin. Immunol.* **2012**, *24*, 310–315.
- (63) Mbow, M. L.; De Gregorio, E.; Valiante, N. M.; Rappuoli, R. New Adjuvants for Human Vaccines. *Curr. Opin. Immunol.* **2010**, *22*, 411–418.
- (64) Mantile, F.; Trovato, M.; Santoni, A.; Barba, P.; Ottonello, S.; De Berardinis, P.; Prisco, A. Alum and Squalene-Oil-in-Water Emulsion Enhance the Titer and Avidity of Anti-A β Antibodies Induced by Multimeric Protein Antigen (1–11)E2, Preserving the Igg1-Skewed Isotype Distribution. *PLoS One* **2014**, *9*, e101474.
- (65) Luxton, R. W.; Thompson, E. J. Affinity Distributions of Antigen-Specific IgG in Patients with Multiple Sclerosis and in

- Patients with Viral Encephalitis. *J. Immunol. Methods* **1990**, *131*, 277–282.
- (66) Zakeri, B.; Fierer, J. O.; Celik, E.; Chittock, E. C.; Schwarz-Linek, U.; Moy, V. T.; Howarth, M. Peptide Tag Forming a Rapid Covalent Bond to a Protein, through Engineering a Bacterial Adhesin. *Proc. Natl. Acad. Sci. U. S. A.* **2012**, *109*, E690–E697.
- (67) Schoene, C.; Bennett, S. P.; Howarth, M. SpyRings Declassified: A Blueprint for Using Isopeptide-Mediated Cyclization to Enhance Enzyme Thermal Resilience. *Methods Enzymol.* **2016**, *580*, 149–167.
- (68) Schoene, C.; Bennett, S. P.; Howarth, M. SpyRing Interrogation: Analyzing How Enzyme Resilience Can Be Achieved with Phytase and Distinct Cyclization Chemistries. *Sci. Rep.* **2016**, *6*, 21151.
- (69) Galimidi, R. P.; Klein, J. S.; Politzer, M. S.; Bai, S.; Seaman, M. S.; Nussenzweig, M. C.; West, A. P.; Bjorkman, P. J. Intra-Spike Crosslinking Overcomes Antibody Evasion by HIV-1. *Cell* **2015**, *160*, 433–446.
- (70) Klein, J. S.; Bjorkman, P. J. Few and Far between: How HIV May Be Evading Antibody Avidity. *PLoS Pathog.* **2010**, *6*, e1000908.
- (71) Khurana, S.; Wu, J.; Verma, N.; Verma, S.; Raghunandan, R.; Manischewitz, J.; King, L. R.; Kpamegan, E.; Pincus, S.; Smith, G.; Glenn, G.; Golding, H. H5N1 Virus-Like Particle Vaccine Elicits Cross-Reactive Neutralizing Antibodies That Preferentially Bind to the Oligomeric Form of Influenza Virus Hemagglutinin in Humans. *J. Virol.* **2011**, *85*, 10945–10954.
- (72) Spohn, G.; Jennings, G. T.; Martina, B. E. E.; Keller, I.; Beck, M.; Pumpens, P.; Osterhaus, A. D.; Bachmann, M. F. A VLP-Based Vaccine Targeting Domain III of the West Nile Virus E Protein Protects from Lethal Infection in Mice. *Virol. J.* **2010**, *7*, 146.
- (73) Schmitz, N.; Beerli, R. R.; Bauer, M.; Jegerlehner, A.; Dietmeier, K.; Maudrich, M.; Pumpens, P.; Saudan, P.; Bachmann, M. F. Universal Vaccine against Influenza Virus: Linking TLR Signaling to Anti-Viral Protection. *Eur. J. Immunol.* **2012**, *42*, 863–869.
- (74) Ura, T.; Okuda, K.; Shimada, M. Developments in Viral Vector-Based Vaccines. *Vaccines* **2014**, *2*, 624–641.
- (75) Bale, J. B.; Gonen, S.; Liu, Y.; Sheffler, W.; Ellis, D.; Thomas, C.; Cascio, D.; Yeates, T. O.; Gonen, T.; King, N. P.; Baker, D. Accurate Design of Megadalton-Scale Two-Component Icosahedral Protein Complexes. *Science* **2016**, *353*, 389–394.
- (76) Butterfield, G. L.; Lajoie, M. J.; Gustafson, H. H.; Sellers, D. L.; Nattermann, U.; Ellis, D.; Bale, J. B.; Ke, S.; Lenz, G. H.; Yehdego, A.; Ravichandran, R.; Pun, S. H.; King, N. P.; Baker, D. Evolution of a Designed Protein Assembly Encapsulating Its Own RNA Genome. *Nature* **2017**, *552*, 415–420.
- (77) Qin, Q.; Yin, Z.; Wu, X.; Haas, K. M.; Huang, X. Valency and Density Matter: Deciphering Impacts of Immunogen Structures on Immune Responses against a Tumor Associated Carbohydrate Antigen Using Synthetic Glycopolymers. *Biomaterials* **2016**, *101*, 189–198.
- (78) Dintzis, R. Z.; Middleton, M. H.; Dintzis, H. M. Studies on the Immunogenicity and Tolerogenicity of T-Independent Antigens. *J. Immunol.* **1983**, *131*, 2196–2203.
- (79) Li, L.; Fierer, J. O.; Rapoport, T. A.; Howarth, M. Structural Analysis and Optimization of the Covalent Association between SpyCatcher and a Peptide Tag. *J. Mol. Biol.* **2014**, *426*, 309–317.
- (80) Douglas, A. D.; Williams, A. R.; Illingworth, J. J.; Kamuyu, G.; Biswas, S.; Goodman, A. L.; Wyllie, D. H.; Crosnier, C.; Miura, K.; Wright, G. J.; Long, C. A.; Osier, F. H.; Marsh, K.; Turner, A. V.; Hill, A. V. S.; Draper, S. J. The Blood-Stage Malaria Antigen PfPR5 Is Susceptible to Vaccine-Inducible Cross-Strain Neutralizing Antibody. *Nat. Commun.* **2011**, *2*, 601–609.
- (81) Keeble, A. H.; Banerjee, A.; Ferla, M. P.; Reddington, S. C.; Anuar, I. N. A. K.; Howarth, M. Evolving Accelerated Amidation by SpyTag/SpyCatcher to Analyze Membrane Dynamics. *Angew. Chem., Int. Ed.* **2017**, *56*, 16521–16525.
- (82) The UniProt Consortium. UniProt: The Universal Protein Knowledgebase. *Nucleic Acids Res.* **2017**, *45*, D158–D169.
- (83) Altschul, S. F.; Madden, T. L.; Schäffer, A. A.; Zhang, J.; Zhang, Z.; Miller, W.; Lipman, D. J. Gapped BLAST and PSI-BLAST: A New Generation of Protein Database Search Programs. *Nucleic Acids Res.* **1997**, *25*, 3389–3402.
- (84) Aida, Y.; Pabst, M. J. Removal of Endotoxin from Protein Solutions by Phase Separation Using Triton X-114. *J. Immunol. Methods* **1990**, *132*, 191–195.

Supporting Information

Engineering a Rugged Nanoscaffold to Enhance Plug-and-Display Vaccination

Theodora U.J. Bruun^{1†}, Anne-Marie C. Andersson^{1†}, Simon J. Draper², and Mark Howarth^{1*}

¹Department of Biochemistry, University of Oxford, South Parks Road, Oxford, OX1 3QU, UK. ²Jenner Institute, University of Oxford, Oxford, OX3 7DQ, UK.

*Correspondence and requests for materials should be addressed to M.H. (email: mark.howarth@bioch.ox.ac.uk).

A

| | | | |
|---------------|-----|--|-----|
| KDPG Aldolase | 1 | MKMEELFKKHKIVAVLRANSVEEAK E KALAVF E GGVHLIEITFTVPDADTV | 51 |
| i301 | 1 | MKMEELFKKHKIVAVLRANSVEEAK K KALAVF L GGVHLIEITFTVPDADTV | 51 |
| mi3 | 1 | MKMEELFKKHKIVAVLRANSVEEAK K KALAVF L GGVHLIEITFTVPDADTV | 51 |
| KDPG Aldolase | 52 | IKELSFLKE K GAIIGAGTVTSVEQ C RKAVESGAEFIVSPHLDEEISQF C KE | 102 |
| i301 | 52 | IKELSFLKE M GAIIGAGTVTSVEQ C RKAVESGAEFIVSPHLDEEISQF C KE | 102 |
| mi3 | 52 | IKELSFLKE M GAIIGAGTVTSVEQ A RKAVESGAEFIVSPHLDEEISQF A KE | 102 |
| KDPG Aldolase | 103 | KGVFYMPGVMTPTELVKAMKLGHTILKLFPGEVVGPQFVKAMKGPFPNVKF | 153 |
| i301 | 103 | KGVFYMPGVMTPTELVKAMKLGHTILKLFPGEVVGPQFVKAMKGPFPNVKF | 153 |
| mi3 | 103 | KGVFYMPGVMTPTELVKAMKLGHTILKLFPGEVVGPQFVKAMKGPFPNVKF | 153 |
| KDPG Aldolase | 154 | VPTGGVNLDNVCEWFKAGVLAVGVGSALVKGTP D EV R EKAKAFVEKIRGCTE | 205 |
| i301 | 154 | VPTGGVNLDNVCEWFKAGVLAVGVGSALVKGTP V EV A EKAKAFVEKIRGCTE | 205 |
| mi3 | 154 | VPTGGVNLDNVCEWFKAGVLAVGVGSALVKGTP V EV A EKAKAFVEKIRGCTE | 205 |

B

| | | | | | |
|--|----|--|--|---|-----|
| | | ↓ | | ↓ | |
| <i>Thermotoga maritima</i> | 71 | TSVEQCRKAVESGAEFIVSPHLDEEISQFCKEKG | | | 104 |
| <i>Thermotoga naphthophila</i> | 69 | TSVEQCRKAVESGAEFIVSPHLDEEISQFCKEKG | | | 102 |
| <i>Treponema phagedenis</i> | 74 | L D A T T A R F A I M N G A R F V V S P A F D K E V A M L C N L Y Q | | | 107 |
| <i>Anaerosphaera aminiphila</i> | 74 | L D S T T A R L A I M N G A K F I V S P S F D E E V A K L C N L Y Q | | | 107 |
| <i>Caldisalibacter kiritimatiensis</i> | 76 | L D S E T A R I A I L S G A Q Y I V S P S F D L K T A K L C N R Y Q | | | 109 |
| <i>Bacillus acidiceler</i> | 76 | L D V T T A R I A I M A G A Q F V V S P A F D E E T A K L C N L Y Q | | | 109 |
| <i>Sebaldella termitidis</i> | 74 | L D S E T A R N A I L S G A T Y I V S P G F D E N T A K L C N R Y C | | | 107 |
| <i>Fusobacterium varium</i> | 76 | L D A A T A R I A I L A G S E F I V S P A F D E E T A K L C N L Y Q | | | 109 |
| <i>Paenibacillus polymyxa</i> | 74 | L E S L T A R I A I L A G A E F V V S P S F E E T A K L C N L Y A | | | 107 |
| <i>Streptococcus didelphis</i> | 71 | M S L E L A K E A I Q A G A S F L V S P H F D K E I A D L A N Q E Q | | | 104 |
| <i>Mesotoga prima</i> | 68 | I T D D Q F S K A V K S G A K Y V V S P H L S E E L A I Q S R A L E | | | 101 |

Figure S1. Alignment and conservation for mi3. (a) Alignment of amino acid sequences for *Thermotoga maritima* KDPG aldolase, i301 and mi3. Residues where there are changes are shown in red. **(b)** Conservation in representative KDPG aldolases at amino acids 76 and 100 (marked with arrows), after a PSI-BLAST search based on the version from *T. maritima*. Residues different from the *T. maritima* sequence are shown in red.

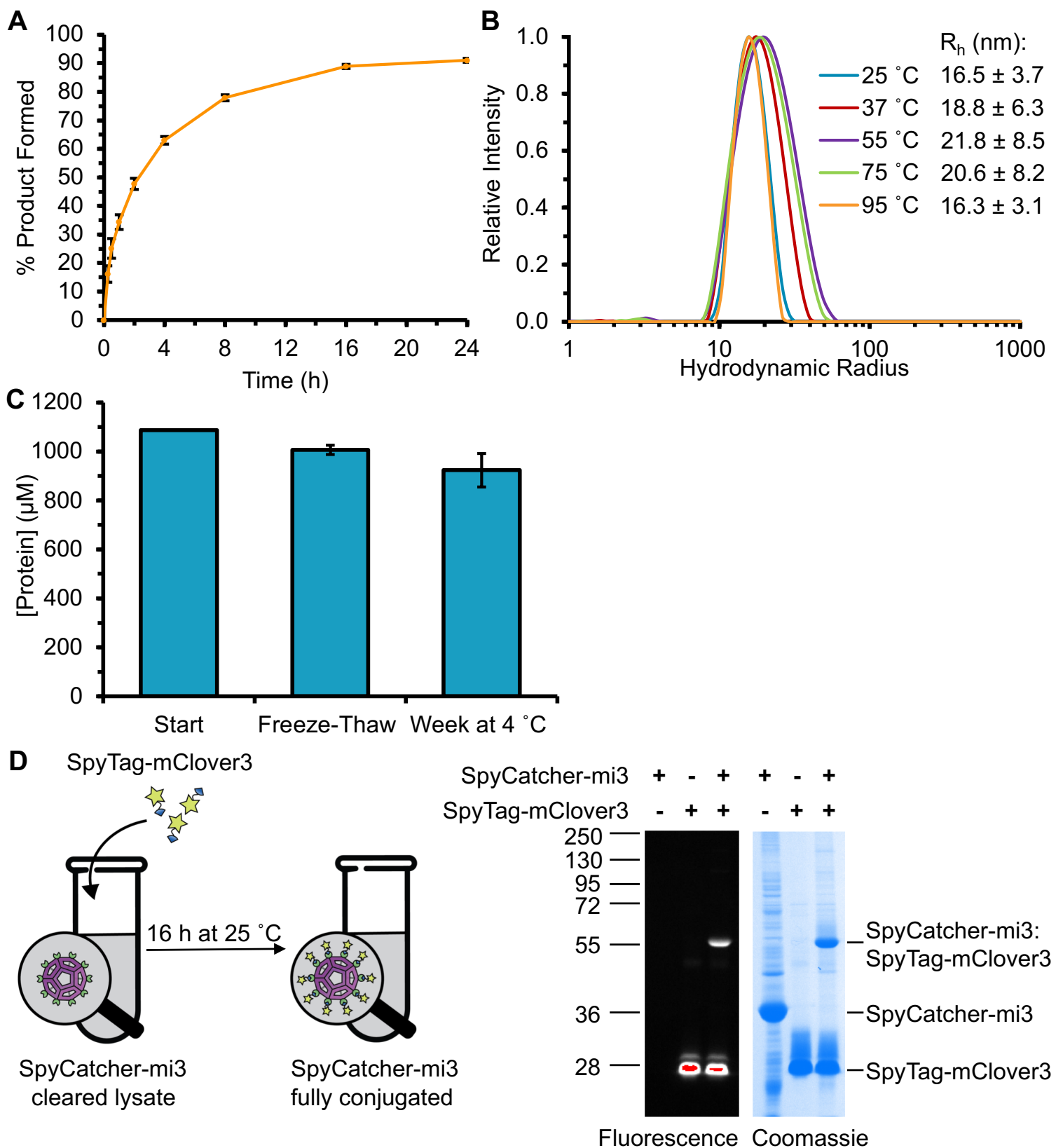


Figure S2. SpyCatcher-mi3 reactivity and stability. (a) Reaction time-course. 5 μM SpyCatcher-mi3 was incubated with 15 μM SpyTag-MBP for the indicated time at 25 $^{\circ}\text{C}$, before analysis by SDS-PAGE with Coomassie staining. (b) VLP integrity following heating. SpyCatcher-mi3 at 30 μM was incubated for 1 h at the indicated temperature. Samples were then centrifuged to remove aggregates, adjusted to 0.125 mg/mL, and measured at 20 $^{\circ}\text{C}$ by DLS. Hydrodynamic radius for each sample is shown. (c) Storage stability. SpyCatcher-mi3 at 1,090 μM underwent one round of freeze-thaw or was stored at 4 $^{\circ}\text{C}$ for 1 week. The sample was centrifuged to remove aggregates and the protein concentration in the supernatant is plotted. (d) SpyCatcher-mi3 could react with antigen directly in cell lysate. Purified antigen (SpyTag-mClover3) was added to cleared lysate from *E. coli* expressing SpyCatcher-mi3 and incubated for 16 h at 25 $^{\circ}\text{C}$. The cleared lysate was then analyzed *via* SDS-PAGE (samples were not boiled) by fluorescence (left) followed by Coomassie staining (right). Data show mean of triplicate \pm 1 s.d.; some error bars were too small to be visible.

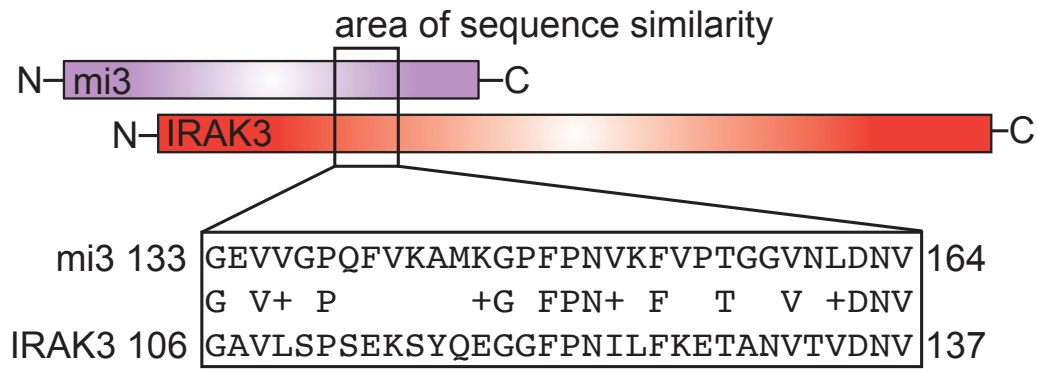
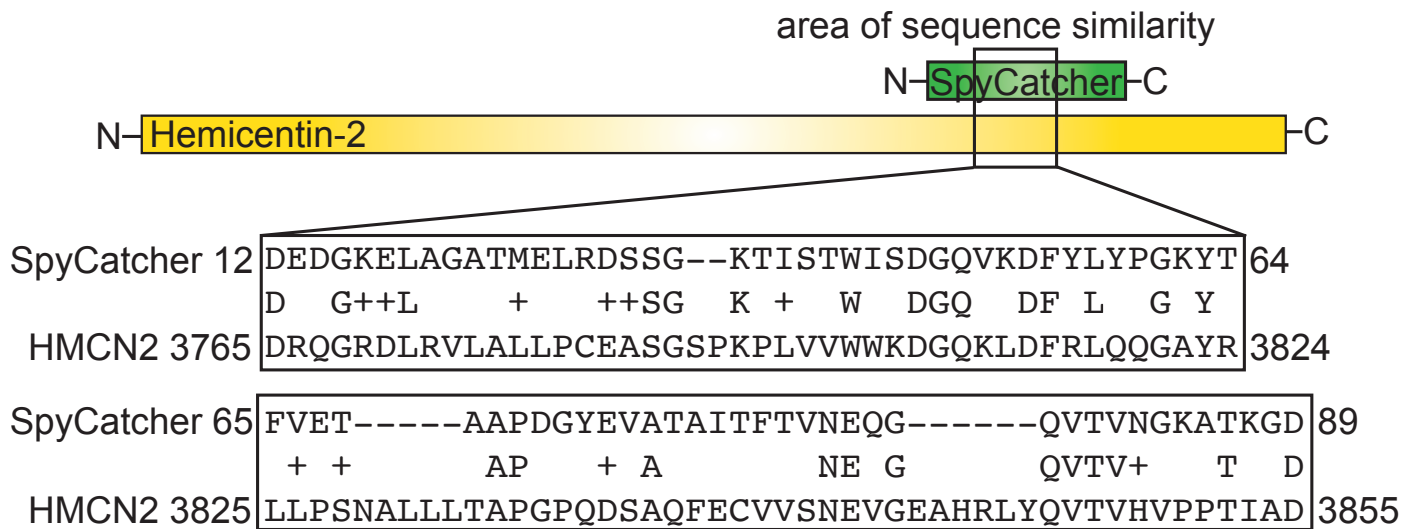
A**B**

Figure S3. Minimal sequence similarity to mi3 or SpyCatcher in the human genome.

Sequence alignment of the top hit after BLAST against the UniProtKB_human database for (a) mi3 and (b) SpyCatcher.